Commensurately modulated structure of $4H_b$-$TaSe_2$ determined by x-ray crystal-structure refinement

Jens Lüdecke* and Sander van Smaalen
Laboratory of Crystallography, University of Bayreuth, D-95440 Bayreuth, Germany

Albert Spijkerman, Jan L. de Boer, and Gerrit A. Wiegers
Department of Chemical Physics, Materials Science Center, University of Groningen, Nijenborgh 4, NL-9747 AG Groningen, The Netherlands

(Received 4 August 1998)

The $(\sqrt{13}a\times\sqrt{13}a\times c)$ superstructure of $4H_b$-$TaSe_2$ at room temperature has been determined by x-ray crystal-structure refinement using (3+2)-dimensional superspace. The resulting modulation has its largest amplitudes for a longitudinal displacement of the Ta atoms in the octahedrally coordinated (*T*) layers, thus leading to a superstructure of hexagram-shaped clusters containing thirteen Ta atoms each. The atoms in the corresponding planes of Se atoms show a transversal modulation, which can be interpreted as the relaxation of these layers to the modulation of the Ta layers. Forming a similar pattern, modulations were found of the atoms in the layers with Ta in trigonal prismatic coordination (*H* layers), with amplitudes of about 1/10 of the sizes of the modulations in the *T* layers. These results confirm the presence of a charge-density wave in the *T* layers, while the modulations of the *H* layer can be assigned to elastic coupling between the two types of layers. The observation of nonzero displacements of the atoms of the *H* layers provides an interpretation for recent observations by scanning tunneling microscope (STM): the superstructure features observed by STM on the *H* layers is a direct consequence of the atomic displacements in this layer. [S0163-1829(99)03306-8]

I. INTRODUCTION

$4H_b$-$TaSe_2$ belongs to the class of layered transition-metal dichalcogenides that show phases with various commensurately and incommensurately modulated structures. The phase transitions are driven by charge-density-wave (CDW) instabilities in the quasi-two-dimensional electron bands on the planes of transition-metal atoms.

Transition-metal dichalcogenides are known for polytypism.[1] The structures are built as a stacking of three-atoms-thick layers TaX_2(X=S, Se), with Ta either in octahedral coordination (*T* layer) or in trigonal-prismatic coordination (*H* layer). $1T$-TaX_2 comprises a simple stacking of *T* layers, $2H$-TaX_2 is a stacking of *H* layers, and $4H_b$-TaX_2 is built as an alternate stacking of *H* and *T* layers.

The space group of the high-temperature structure of $4H_b$-$TaSe_2$ is $P6_3/mmc$, with lattice parameters $a=b=3.455$ Å and $c=25.15$ Å (Fig. 1).[2] This structure persists at all temperatures as basic or average structure. Below around 600 K a CDW develops, resulting in an incommensurately modulated structure. This phase locks into a commensurate $(\sqrt{13}a\times\sqrt{13}a\times c)$ superstructure at 410 K. Below around 75 K a second CDW develops, again with an incommensurate modulation. An overview of the characteristic parameters of the different phases is given in Table I. Previous x-ray-scattering experiments have confirmed that the commensurate CDW at room temperature is located in the *T* layers.[3] However, the analysis by Moret and Tronc[3] was incomplete, as only an average value was determined for the modulation amplitudes of the atoms in the *T* layer. A modulation of the *H* layers was not considered.

In this paper a complete determination is presented of the $(\sqrt{13}a\times\sqrt{13}a\times c)$ superstructure of $4H_b$-$TaSe_2$ at room temperature. In agreement with Moret and Tronc we found large modulation amplitudes for the atoms of the *T* layers. However, significant modulation amplitudes were also found for the atoms of the *H* layers, with values of about 1/10 of those of the atoms in the *T* layers.

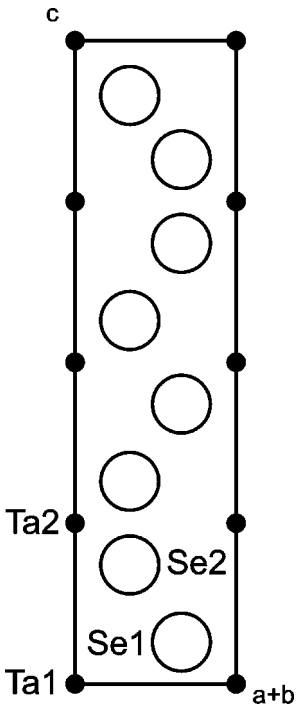

FIG. 1. [110] section of one unit cell of the basic structure of $4H_b$-$TaSe_2$.

TABLE I. The CDW states of $4H_b$-$TaSe_2$ at different temperatures as reported by Wilson *et al.* (Ref. 7).

T (K)	CDW state	Layers involved	Modulation wave vector
>600	Normal		
410–600	Incommensurate	Octahedral	$\mathbf{q}^T=0.265\mathbf{a}^*$
75–410	Commensurate	Octahedral	$q^T=0.277a^*$; α,β superlattices
<75	Incommensurate	Trigonal prismatic	$\mathbf{q}^H=\mathbf{a}^*/3(1+\delta)$, at 10 K, $\delta=0.04$
	Commensurate	Octahedral	$q^T=0.277a^*$; α,β superlattices

The results are discussed in terms of elastic coupling between the different atoms. Employing the superspace description, the superstructure in $4H_b$-$TaSe_2$ is compared with the incommensurate modulation in $1T$-TaS_2 at room temperature.

The discovery of small modulation amplitudes in the H layers strongly suggests an alternative interpretation for the scanning tunneling microscope (STM) experiments on $4H_b$-TaS_2.[4–6] The observation of a $(\sqrt{13}a\times\sqrt{13}a)$ CDW modulation in the STM images of the H layer is more likely a true structural effect than it is due to tunneling of electrons from the T layer through the unoccupied states of the H layer as suggested by Han *et al.*[4] and more recently by Ekvall *et al.*[6]

II. EXPERIMENT

Single crystals of $4H_b$-$TaSe_2$ samples have been prepared using the gas transport technique in evacuated quartz ampoules. X-ray-diffraction experiments were performed on a Nonius CAD4F diffractometer with Mo-K_α radiation ($\lambda=0.710\,73$ Å). A rather small crystal was chosen of size $0.22\times0.28\times0.005$ mm^3 because of the high absorption coefficient ($\mu=699\,\mathrm{cm}^{-1}$). Lattice parameters of the average structure were obtained from the setting angles of 25 reflections in the range $25°<\Theta<34°$, resulting in $a=b=3.4552(2)$ Å and $c=25.1495(13)$ Å. These values are in agreement with those determined by Ref. 2, taking in account the standard deviations of the data. The space group of the average structure is $P6_3/mmc$. However, the modulation leads to a loss of the mirror planes parallel to $\mathbf{c}$.[3] Therefore the symmetry is reduced to $P6_3/m$ at room temperature.

As is known from electron microscopy, the CDW transition at 600 K results in a twinned crystal, with domains of the superstructure in two orientations.[7] The diffraction pattern corresponds to a reciprocal lattice in two orientations, related by a missing symmetry element. The main reflections of the two domains overlap completely, but the satellites (superstructure reflections) occur at different positions (pseudomerohedral twinning). Using one reciprocal lattice for the main reflections, the satellites of the first domain can be described by the modulation wave vectors

$$\mathbf{q}_{1\alpha}=(3\mathbf{a}_0^*+\mathbf{b}_0^*)/13, \tag{1}$$

$$\mathbf{q}_{2\alpha}=(-\mathbf{a}_0^*+4\mathbf{b}_0^*)/13, \tag{2}$$

while the satellites of the second domain define modulation wave vectors

$$\mathbf{q}_{1\beta}=(4\mathbf{a}_0^*-\mathbf{b}_0^*)/13, \tag{3}$$

$$\mathbf{q}_{2\beta}=(\mathbf{a}_0^*+3\mathbf{b}_0^*)/13. \tag{4}$$

Figure 2 displays a picture of reciprocal space of the twinned crystal. Each main Bragg reflection is surrounded by three satellites of first order and three satellites of second order of each of the two domains. Due to the commensurate character higher-order satellites do not occur. Indexing of all reflections of one domain can be done by five integers. Indexing of the complete diffraction pattern of a twinned crystal requires seven integers.

Intensity data were measured at room temperature for the main reflections as well as for the satellites of both domains of a single crystal. All reflections were measured up to a $\Theta=30°$, corresponding to 19 623 data points. Measured intensities were corrected for Lorentz and polarization effects, and for absorption (transmission factors were between 0.07 and 0.69). The data exhibited Laue symmetry $6/m$. Averaging according to this point group resulted in a data set of a total of 2424 unique reflections. Using a criterion for observed reflections of $I>3\sigma(I)$ the data reduced to 487 observed main reflections and 1108 observed first- and second-order satellites in the final data set.

The symmetry of the superstructure can be characterized by a superspace group or by a supercell space group. As was confirmed by subsequent refinements, the structure is centrosymmetric. Then, the only superspace group compatible with the average structure, the observed twinning, and with the diffraction symmetry is $P6_3/m(\alpha,\beta,0)$. The values $\alpha=\frac{3}{13}$ and $\beta=\frac{1}{13}$ are determined by Eq. (2). For a given modulation function, the supercell structure and supercell symmetry depend on the section chosen along the fourth and fifth superspace axes. The possibilities for the supercell space group are $P6_3/m$, $P2_1/m$, and Pm. Deviations from

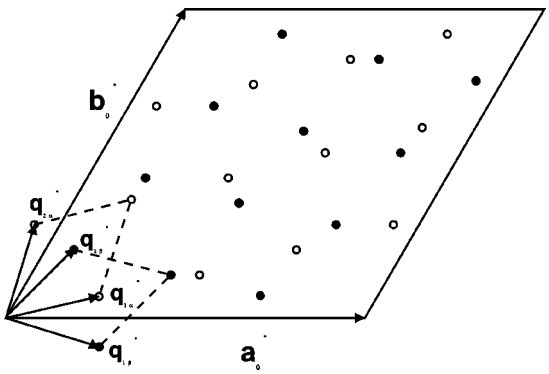

FIG. 2. The section $l=0$ of reciprocal space, showing one unit cell of the reciprocal lattice of the basic structure $4H_b$-$TaSe_2$, together with the positions of the satellite reflections originating in either of the two domains.

the highest possible symmetry, while retaining Laue symmetry $6/m$, are only possible when multiple twinning occurs. Such deviations could not be detected, and the supercell space group was chosen as $P6_3/m$.

III. STRUCTURE DETERMINATION

In a first step the basic structure was refined against the main reflections. Initial coordinates were those reported by Moret and Tronc.[3] Smooth convergence was obtained towards $R_F=0.071(wR_{F^2}=0.109)$, resulting in the expected structure. Anomalously large temperature parameters indicated that the true structure was modulated. These calculations and all subsequent refinements were performed with the program system JANA96.[8]

Special methods for structure solution were not applied to determine the modulation parameters. The set of parameters corresponding to the best fit was obtained by refinements using different sets of starting parameters. The superstructure was described as a commensurately modulated structure of the basic structure with modulation functions for each of the four independent atoms defined by their Fourier series:

$$u_\alpha^\mu=\sum_{n_1}\sum_{n_2} A^\mu_{n_1,n_2,\alpha}\sin(2\pi n_1\overline{x_4}+2\pi n_2\overline{x_5}) + B^\mu_{n_1,n_2,\alpha}\cos(2\pi n_1\overline{x_4}+2\pi n_2\overline{x_5}), \quad (5)$$

where (n_1,n_2) defines the order of the harmonic $\alpha=x,y,z$ and μ indicates the atom. The commensurateness determines that only a finite number of combinations (n_1,n_2) are independent, such that the number of parameters in the modulation approach is equal to the number of parameters in the supercell approach. All independent parameters were taken into account.

The additional superspace coordinates $\overline{x_4}$ and $\overline{x_5}$ are related to the basic structure coordinates by

$$\overline{x_4}=\mathbf{q}_1\cdot\mathbf{r}+t_1, \quad (6)$$

$$\overline{x_5}=\mathbf{q}_2\cdot\mathbf{r}+t_2. \quad (7)$$

It should be noted that for a commensurate structure the structure in physical space and its symmetry depend on the values of the starting phase (t_1,t_2) of the modulation. In accordance with the symmetry $P6_3/m(\alpha,\beta,0)$ we have fixed these values at $(t_1,t_2)=(0,0)$.

Restrictions on the components of the modulation functions follow from site symmetries of the atoms on special positions. The *T* layer contains one crystallographically independent Ta atom with site symmetry $\overline{3}$, and one independent Se atom with site symmetry 3. For the *H* layer, Ta2 has site symmetry $\overline{6}$ and Se2 has site symmetry 3. The number of modulation amplitudes is reduced from 36 independent parameters towards 6 parameters for Ta1, from 36 parameters towards 8 parameters for Ta2, and from 36 parameters towards 12 parameters in the case of both Se atoms. The restrictions are summarized in Table II. Together with 1 parameter for each Se atom describing the *z* coordinate of the basic structure position, a total number of 40 independent positional parameters were varied in the refinements of the modulated structure. This gives a complete description of all degrees of freedom corresponding to the $(\sqrt{13}a\times\sqrt{13}a\times c)$ superstructure.

TABLE II. Symmetry restrictions on the parameters of the modulation functions in the superspace description of the $(\sqrt{13}a\times\sqrt{13}a\times c)$ superstructure of $4H_b$-$TaSe_2$.

Point group $\overline{3}$, Ta1 atom at (0,0,0)

$$A^x_{-n_1-n_2,n_1}=-A^x_{n_1,n_2}+A^x_{-n_2,n_1+n_2}$$
$$A^y_{n_1,n_2}=A^x_{n_1+n_2,-n_1}$$
$$A^z_{n_1,n_2}=-A^z_{n_1+n_2,-n_1}$$
$$B^x_{n_1,n_2}=B^y_{n_1,n_2}=B^z_{n_1,n_2}=0$$

Point group $\overline{6}$, Ta2 atom at (0,0,1/4)

$$A^x_{-n_1-n_2,n_1}=-A^x_{n_1,n_2}+A^x_{-n_2,n_1+n_2}$$
$$A^y_{n_1,n_2}=A^x_{n_1+n_2,-n_1}$$
$$B^x_{-n_1-n_2,n_1}=-B^x_{n_1,n_2}-B^x_{-n_2,n_1+n_2}$$
$$B^y_{n_1,n_2}=-B^x_{n_1+n_2,-n_1}$$
$$A^z_{n_1,n_2}=B^z_{n_1,n_2}=0$$

Point group 3, Se atoms at (1/3,2/3,z)

$$A^x_{-n_1-n_2,n_1}=-A^x_{n_1,n_2}+A^x_{-n_2,n_1+n_2}$$
$$A^y_{n_1,n_2}=A^x_{n_1+n_2,-n_1}$$
$$A^z_{n_1,n_2}=-A^z_{n_1+n_2,-n_1}$$
$$B^x_{-n_1-n_2,n_1}=-B^x_{n_1,n_2}-B^x_{-n_2,n_1+n_2}$$
$$B^y_{n_1,n_2}=-B^x_{n_1+n_2,-n_1}$$
$$B^z_{n_1,n_2}=B^z_{n_1+n_2,-n_1}$$

Special attention was required for the problem of twinning. Intensities of the satellites of the individual domains were available directly from the experiment. The ratio of the volume fractions of the two domains (f_v) then follows as the ratio of the intensities of corresponding satellite reflections. Averaged over all satellites, a value was obtained of $f_v=1.58$. The main reflections of the two domains overlap, and only a sum of two intensity values was available. A main reflection (h,k,l) of the first domain coincides with a main reflection $(k,h,\overline{l})$ of the second domain. These reflections are not equivalent in $6/m$ symmetry. A classical approach to the twinning problem is to determine the intensities of the individual reflections from f_v and the measured values for overlapping reflections. However, this aproach becomes increasingly inaccurate when f_v approaches 1, and it fails completely when $f_v=1$.

An alternative approach to the twinning problem is to refine the structural parameters, scale factor, and the volume ratio of the domains against the experimental intensities directly. To achieve this, it is necessary to build the appropriate sum of calculated intensities for each individual data point. All measured data can then be included into a single refinement. In the present case, this would require an indexing of the diffraction pattern with seven integers.[9] As it is presently not possible to use more than six indices in the program JANA, we could not use this method directly. Instead, we used the approximation that the reflections (h,k,l) and $(k,h,\overline{l})$ will not be much different (note that they are equivalent by symmetry in the basic structure), expressed by the assumption that the effect of the modulation will be equal

TABLE III. Partial R factors and number of reflections used in the refinement of $4H_b$-$TaSe_2$.

Reflection group	No. observed	R_F	wR_F^2
Main	487	5.84	13.75
Satellites	1108	9.69	10.53
All	1595	7.13	12.32

for the two reflections in each pair. Then we can restrict the experimental data to main reflections and the satellites of one domain, thus requiring only five indices. The effect of twinning is then entirely contained in individual scale factors for the main reflections and the satellites. This description with the scale factors f_{main} and f_{sat} was used here in the refinements (the scale factor is defined to multiply the calculated intensity values).

Two pronounced minima of the R factor were found, corresponding to modulations of either the T layers or the H layers. The fit of the structure with the stronger modulation in the T layers was slightly better ($R=0.0713$) than the fit with the stronger modulation in the H layers ($R=0.0787$). Additional support for the true structure as the one with the stronger modulation in the T layers was provided by the partial R factors of the main reflections. For modulation in the H layers $R(\text{main})=0.0688$ was significantly higher than for modulation in the T layers [$R(\text{main})=0.0584$]. Next to providing the best fit, strongest support for the correct structure comes from the fact that the structure with the largest modulation in the T layers was the only one corresponding to a stable refinement of all independent parameters. Contrary, the refinement with the largest modulation in the H layers was only stable when the modulation amplitudes of the T layers were fixed at small values. The resulting R factors for our best fit are listed in Table III. The parameters of the final structure model are summarized in Tables IV–VIII.

The ratio of the scale factor of the main reflections and the scale factor of the satellites was found as $f_{main}/f_{sat}=2.77(3)$. For the given ratio of volume fractions of the domains f_v, a theoretical value follows as $(f_{main}/f_{sat})^{\text{th}}=(1+f_v)/f_v=1.63$. Assuming that the main reflections have intensities as expected, it can be derived that the actually observed intensities of the satellite reflections are smaller by a factor of 0.588 than would follow from the structure model. The only explanation we can give for this discrepancy is that the superstructure is only partially ordered, while the average structure remains fully ordered. For example, it could be that the center of the hexagram-shaped clusters in consecutive layers is at different positions (x,y), contrary to the structure model that assumes perfect coherence between different layers. Moret and Tronc observed a discrepancy in the ratio of scale factors of similar size.[3] However they incorrectly assumed that the ratio of scale factors would depend on the amount of coherence between the two types of domains. That is true for the maximum value of the Bragg reflections. But for integrated intensities of Bragg reflections, the values are independent of the amount of coherence between the two types of domains. Therefore the disorder proposed here pertains to disorder within a single domain, and it is not related to a possible disorder in the stacking of the two types of domains. No evidence can be extracted from the present results or from Ref. 3 pertaining to a possible coherence between the two types of domains.

TABLE IV. Parameters of the basic structure of $4H_b$-$TaSe_2$ after refinement with two harmonics for all atoms. Given are the fractional coordinates of the atoms and their temperature parameters U_{ij} in Å^2. Symmetry determines that $U_{13}=U_{23}=0$, and that $U_{22}=U_{11}=2U_{12}$. Standard deviations are given in parentheses.

Atom	Wyckoff position	x	y	z	U_{11}	U_{33}
Ta1	$2a$	0	0	0	0.0031(2)	0.0026(3)
Ta2	$2b$	0	0	1/4	0.0048(2)	0.0074(3)
Se1	$4f$	1/3	2/3	0.06569(4)	0.0059(2)	0.0026(5)
Se2	$4f$	1/3	2/3	0.68400(3)	0.0041(2)	0.0091(3)

TABLE V. Modulation amplitudes for atom Ta1 for the final refinement. The amplitudes according to Eq. (5) are given in Å along the coordinate axes. Parameters without standard deviation are dependent on other parameters. The parameters B_{n_1,n_2} are equal to zero by symmetry.

$n1,n2$	$A^x_{n_1,n_2}$	$A^y_{n_1,n_2}$	$A^z_{n_1,n_2}$
1,0	−0.1813(7)	−0.0892	0.0537(21)
0,1	−0.0921(5)	−0.1813	−0.0537
−1,1	0.0892	−0.0921	0.0537
1,1	0.0966(6)	−0.0174	−0.0158(49)
−1,2	0.1141(6)	0.0966	0.0158
−2,1	0.0174	0.1141	−0.0158

IV. DISCUSSION

A. Modulations of the T layers

The largest modulation amplitudes were found for Ta1 in the T layers with amplitudes of secondary importance for the Se atoms in the T layers. The modulation of Ta1 was found to be mainly parallel to the plane of the layers (Table V), and its phasing is such that clusters occur containing 13 Ta atoms each. The center of the clusters form the $(\sqrt{13}\times\sqrt{13})$ supercell, rotated by 13°54′ relative to the unit cell of the unmodulated structure (Fig. 3). All these features can be considered evidence that the modulation is driven by a CDW located on the Ta atoms of the T layers.

Because the modulation is commensurate, the superstructure can be studied by the analysis of positions of the atoms,

TABLE VI. Modulation amplitudes for atom Ta2. $A^z_{n_1,n_2}=B^z_{n_1,n_2}=0$ by symmetry.

$n1,n2$	$A^x_{n_1,n_2}$	$A^y_{n_1,n_2}$	$B^x_{n_1,n_2}$	$B^y_{n_1,n_2}$
1,0	0.0113(5)	0.0098	0.0061(34)	−0.0017
0,1	0.0015(6)	0.0113	−0.0078(52)	−0.0061
−1,1	−0.0098	0.0015	0.0017	0.0078
1,1	−0.0014(7)	−0.0002	−0.0044(66)	0.0212
−1,2	−0.0011(5)	−0.0014	0.0256(61)	0.0044
−2,1	0.0002	−0.0011	−0.0212	−0.0256

TABLE VII. Modulation amplitudes for atom Se1.

$n1,n2$	$A^x_{n_1,n_2}$	$A^y_{n_1,n_2}$	$A^z_{n_1,n_2}$	$B^x_{n_1,n_2}$	$B^y_{n_1,n_2}$	$B^z_{n_1,n_2}$
1,0	−0.0424(11)	−0.0141	−0.0124(13)	−0.0188(11)	−0.0046	0.0715(12)
0,1	−0.0282(13)	−0.0424	0.0124	0.0142(13)	0.0188	0.0715
−1,1	0.0141	−0.0282	−0.0124	0.0046	−0.0142	0.0715
1,1	0.0127(14)	−0.0050	0.0309(15)	0.0185(10)	0.0067	−0.0103(15)
−1,2	0.0176(12)	0.0127	−0.0309	−0.0118(13)	−0.0185	−0.0103
−2,1	0.0050	0.0176	0.0309	−0.0067	0.0118	−0.0103

of the bond lengths, and of the variations of the coordinations of the atoms within one unit cell of the superlattice (Fig. 3 and Table IX). However a concise representation of these variations is provided by the so-called *t* plots.[10] Due to the periodicity along the fourth and fifth superspace coordinate, all information about the structure is contained in an interval of width 1 in both t_1 and t_2 [Eq. (7)]. For incommensurately modulations any pair (t_1,t_2) corresponds to a value of $(\overline{x_4},\overline{x_5})$ somewhere in the structure. In contrast, for commensurate modulations only certain values of (t_1,t_2) are allowed. In the present case the superstructure is described by a 13-fold supercell, and accordingly only 13 points (t_1,t_2) within one unit cell actually are realized in physical space. Presently, physical space was chosen as the section $(t_1,t_2)=(0,0)$, and the 13 points describing displacements of atoms realized in the structure are given in Fig. 4.

The *t* plots allow the direct comparison of commensurate and incommensurate modulations of varying superperiod. Previously, we have characterized the specific nature of the incommensurate modulation in the nearly commensurate state of $1T$-TaS_2 by *t* plots of the distances between neighboring Ta atoms within one layer.[11] Here the corresponding plots are given for the commensurate modulation of the *T* layers in $4H_b$-$TaSe_2$ (Figs. 4–7).

Figure 4 displays the distance between the neighboring Ta atoms at (0,0,0) and (1,0,0) as a function of (t_1,t_2). The true distance between Ta(0,0,0) and Ta(1,0,0) appears at $t_1=t_2=0$. It can be easily seen that this distance is the global minimum over all *t* values. Other *t* values correspond to the distances between neighbors Ta(n_1,n_2,n_3) and Ta(n_1+1,n_2,n_3). For example $(t_1,t_2)=(3/13,-1/13)$ corresponds to the distance between Ta(1,0,0) and Ta(2,0,0), which appears close to the global maximum. The same analysis can be applied to the *t* dependence of the distances between the atoms Ta(0,0,0) and Ta(1,1,0) and the distances between the atoms Ta(1,0,0) and the Ta(1,1,0) (Figs. 5 and 6). In all three cases the next-neighbor distance is close to the global minimum for $t_1=t_2=0$. By varying t_1,t_2 all distances to neighboring Ta atoms can be estimated. As a result all these neighboring Ta atoms form a star-shaped cluster of 13 atoms. To investigate the absolute modulation of the Ta atoms the magnitude of the displacement in x,y direction is plotted in Fig. 7. The $\bar{3}$ site symmetry of the Ta atom of the octahedral layer implies a sixfold symmetry in the x_4,x_5 superspace as can be easily seen in the plot. At $t_1=t_2=0$ the displacement relative to the unmodulated structure is zero as to be expected for Ta clusters centered around the Ta(0,0,0) atom. The magnitude of the x,y modulation for the neighboring atoms of Ta(0,0,0) is equal in size and close to the maximum of displacements, which is also in agreement with the proposed hexagram-shaped cluster.

Comparison of the sets of plots with the corresponding ones of incommensurately modulated $1T$-TaS_2 show striking similarities between the modulations of these layers in the two different compounds, indicating that the nature of the CDW is similar in these compounds.

The superstructure of the *T* layer is also similar to the superstructure of $1T$-$TaSe_2$. The Ta-Ta distances within a cluster are found as 3.227 Å and 3.357 Å in $4H_b$-$TaSe_2$. These values are equal to those within the Ta clusters in $1T$-$TaSe_2$ [3.22 Å and 3.34 Å (Ref. 12)].

The correlations between the displacements of the Ta1 atoms and neighboring Se atoms can be obtained by comparing the *t* plots of the Ta-Ta distances with the *t* plot of the *z* displacement of Se1 (Fig. 8). Note that the major modulation amplitudes of Se1 are along **c**, perpendicular to the layers (Table VII). In complete accordance with the results on $1T$-TaS_2, it follows that Se is displaced towards the center of the layer when the nearest Ta atoms have moved apart, and that Se is displaced away of the center of the layer when between Ta atoms a shorter than average bond exists.

B. Three-dimensional order of the CDW

In their analysis of x-ray diffraction experiments, Moret and Tronc[3] assumed that the modulation amplitudes of the

TABLE VIII. Modulation amplitudes for atom Se2.

$n1,n2$	$A^x_{n_1,n_2}$	$A^y_{n_1,n_2}$	$A^z_{n_1,n_2}$	$B^x_{n_1,n_2}$	$B^y_{n_1,n_2}$	$B^z_{n_1,n_2}$
1,0	0.0060(11)	0.0031	0.0039(13)	0.0003(11)	−0.0008	0.0059(13)
0,1	0.0029(13)	0.0060	−0.0039	−0.0011(12)	−0.0003	0.0059
−1,1	−0.0031	0.0029	0.0039	0.0008	0.0011	0.0059
1,1	0.0005(15)	0.0010	−0.0020(16)	−0.0008(11)	−0.0004	0.0021(16)
−1,2	−0.0005(12)	0.0005	0.0020	0.0004(13)	0.0008	0.0021
−2,1	−0.0010	−0.0005	−0.0020	0.0004	−0.0004	0.0021

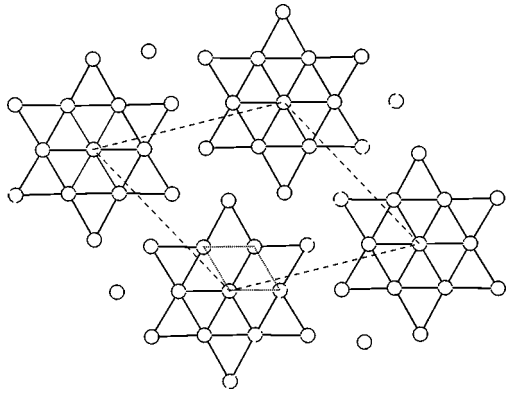

FIG. 3. Section of the superstructure at $z=0$, through the plane of Ta1 atoms. Clusters of 13 atoms are indicated. The superlattice is formed by the centers of the clusters as indicated by dashed lines.

atoms in the *H* layers are zero. Although in the present study the values of the modulation amplitudes of these atoms have been found to be much smaller than the modulations in the *T* layers, the participation of the *H* layer in the modulation is essential to understand the three-dimensional (3D) order of the CDW.

In $1T$-TaS_2 there are only *T* layers present, and neighboring layers are equivalent by translation symmetry. The contact between layers is through their S atoms, and it was observed by analyzing *t* plots that a *z* displacement of S away from the center of the layer corresponded to a *z* displacement towards the center of its layer of the neighboring S atom in the next layer. This phase relation between modulations of different layers was the result of the commensurate component $q_z=\frac{1}{3}$ of the modulation wave vectors.

In $4H_b$-$TaSe_2$ the q_z components of the modulation wave vectors are zero, and the phase relation between consecutive *T* layers is different than in $1T$-TaS_2. However, the basic structures of $1T$-TaS_2 and $4H_b$-$TaSe_2$ are different too, and *T* layers are separated by *H* layers in the latter compound. By comparing *t* plots the correlations become apparent between the *z* displacements of Se1 and Se2 (Figs. 8 and 9). Se2 moves in accordance with Se1, such that each *H* layer is squeezed between the neighboring *T* layers. This phase relation requires a component $q_z=0$, exactly as is found in the

TABLE IX. Coordinates of all atoms in an asymmetric part of the commensurate ($\sqrt{13}\times\sqrt{13}$) supercell, as were derived from the basic structure positions and the modulation functions.

Atom	*x*	*y*	*z*
Ta1-1	0.0	0.0	0.0
Ta1-2	0.0695	0.2867	0.00003
Ta1-3	0.1519	0.6347	0.00401
Ta2-1	0.0	0.0	1/4
Ta2-2	0.0746	0.3068	1/4
Ta2-3	0.1570	0.6154	1/4
Ta2-4	0.3116	0.2321	1/4
Ta2-5	0.5366	0.1516	1/4
Se1-1	2/3	1/3	0.06147
Se1-2	0.1241	0.1750	0.07060
Se1-3	0.3540	0.1027	0.06905
Se1-4	0.5929	0.0281	0.06198
Se1-5	0.1979	0.4842	0.06254
Se2′-1	1/3	2/3	0.18350
Se2′-2	0.1803	0.0513	0.18460
Se2′-3	0.0257	0.4363	0.18380
Se2′-4	0.2569	0.3597	0.18366
Se2′-5	0.4875	0.2820	0.18408

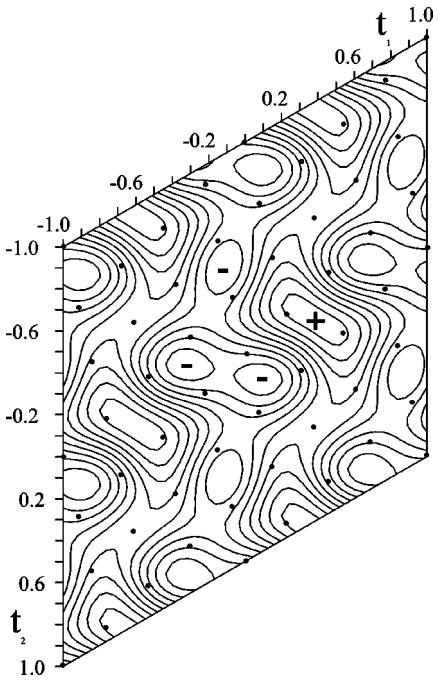

FIG. 4. Distance between Ta(0,0,0) and Ta(1,0,0) as a function of (t_1,t_2). A total of four unit cells are shown. The contour lines are at intervals of 0.1 Å. The plus and minus signs indicate the maxima and minima in the plot. Included as dots are the allowed (t_1,t_2) values for a commensurate ($\sqrt{13}\times\sqrt{13}$) supercell.

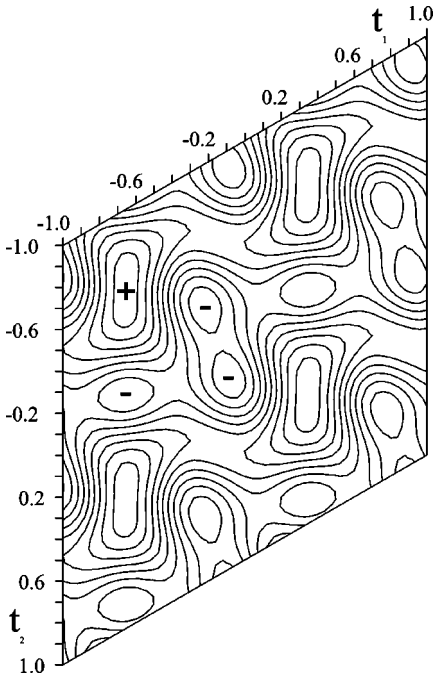

FIG. 5. Distance between Ta(0,0,0) and Ta(1,1,0) as a function of (t_1,t_2). The contour lines are at intervals of 0.1 Å.

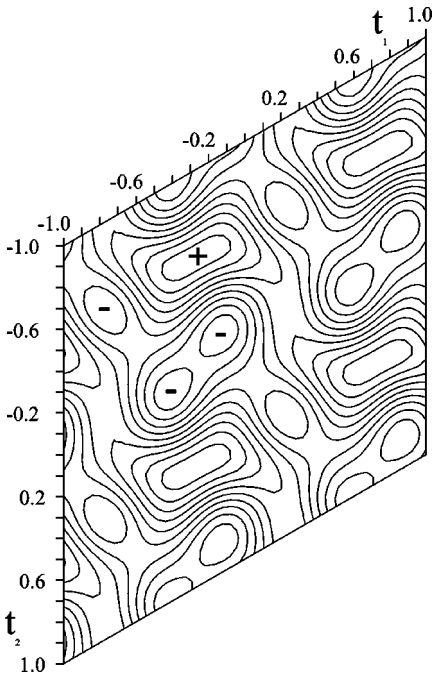

FIG. 6. Distance between Ta(1,0,0) and Ta(1,1,0) as a function of (t_1,t_2). The contour lines are at intervals of 0.1 Å.

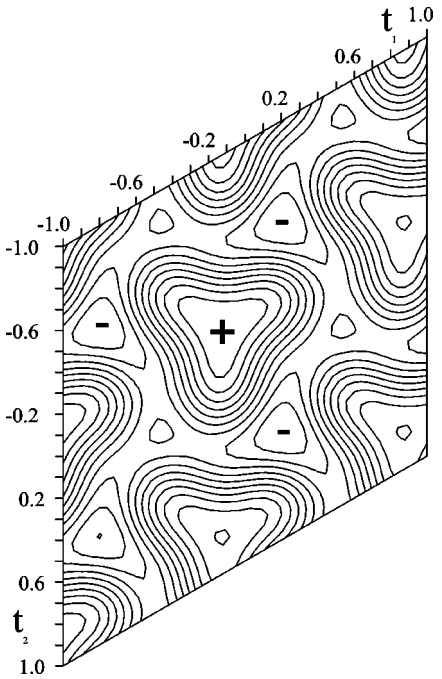

FIG. 8. Values of the z displacement of the Se1 atom at (1/3,2/3,0.066) as a function of (t_1,t_2). The contour lines are at intervals of 0.035 Å.

x-ray scattering. The difference in 3D order of the CDW in $1T$-TaS_2 and $4H_b$-$TaSe_2$ thus is governed by the presence of the H layers in the latter compound.

No indications for disorder were found in the analysis of the structure of $1T$-TaS_2. For $4H_b$-$TaSe_2$ it was presently found that there is disorder in the location of the CDW between different layers. Again these differences can be understood from the intermediate H layers. In $1T$-TaS_2 the coupling between neighboring T layers is relatively strong and good 3D order results. The intermediate H layers determine that the coupling between consecutive T layers in $4H_b$-$TaSe_2$ is relatively weak, apparantly resulting in partial disorder. This interpretation is further supported by the smallness of the modulation in the H layers.

C. Consequences for the interpretation of STM

All polytypes MX_2 comprised of layers MX_2 bonded to each other by weak van der Waals bonds. They cleave across

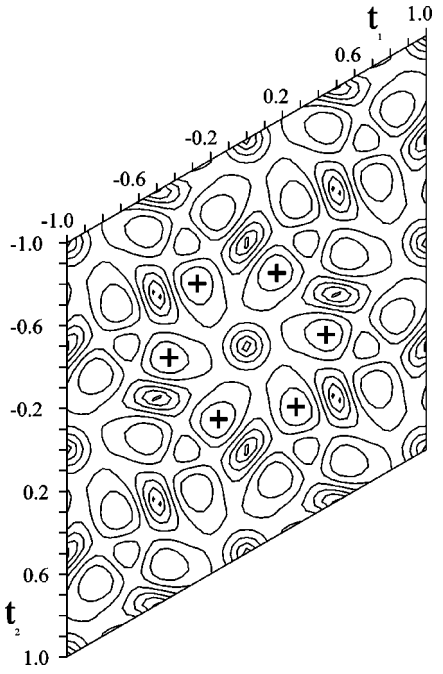

FIG. 7. Absolute values of the x,y displacement of the Ta atom at (0,0,0) as a function of (t_1,t_2). The contour lines are at intervals of 0.05 Å.

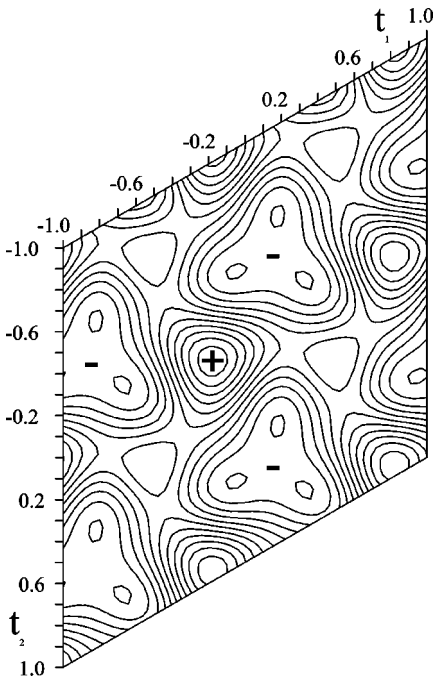

FIG. 9. Values of the z displacement of the Se2′ atom at (2/3,1/3,0.18) as a function of (t_1,t_2). The contour lines are at intervals of 0.0035 Å.

the van der Waals gap, thus exposing layers of S or Se atoms. Consequently STM images the sheets of chalcogen atoms, and it does not see the Ta atoms directly.

In a first approximation the pictures obtained by STM display the local density of states of the *X* atom sheet that correspond to the *z* displacements of these atoms caused by the CDW. This idea was confirmed by electronic band-structure calculations on the commensurate superstructure of $1T$-TaX_2,[13] and the comparison of these calculations with STM experiments. For incommensurate $1T$-TaS_2, a simulated STM image was generated based on the *z* displacements of the *S* atoms determined by x-ray structural analysis, and it was shown that this simulated image was in complete accordance with STM on this phase.[11,14]

The two different layers in $4H_b$-TaX_2 lead to two different surfaces of *X* atoms. STM images of the *T* layers of $4H_b$-TaS_2 clearly showed the $(\sqrt{13}a\times\sqrt{13}a)$ superstructure at all bias voltages of the substrate.[4,5] STM on $4H_b$-$TaSe_2$ was performed with a small negative bias voltage only, and the image of the *T* layer did show a strong effect due to the $(\sqrt{13}a\times\sqrt{13}a)$ superstructure.[15] Again, the pattern of positive and negative *z* displacements of the tip in STM displays the local density of states of the chalcogen sheet that corresponds to the pattern of positive and negative *z* displacements of the Se atoms as determined in x-ray diffraction.

The STM images of the *H* layers of $4H_b$-TaX_2 are more complicated. For $4H_b$-TaS_2 and with a negative bias a superstructure was not visible in STM, while at positive biases a superstructure was found, with the amplitude increasing for increasing bias.[4,6] This effect was explained by tunneling of electrons through unoccupied states of the *H* layer towards the unoccupied states of the *T* layer carrying the CDW.[4,6] The possibility of tunneling in the reverse direction was excluded by assuming screening due to the occupied states of the *H* layers. For STM on the *H* layers of $4H_b$-$TaSe_2$ a weak effect was observed due to the $(\sqrt{13}a\times\sqrt{13}a)$ superstructure at a small negative bias and at a low temperature of 4.2 K.[15] Taking into account that thermal broadening of the density of states at the Fermi level is very small at these low temperatures, tunneling obviously cannot explain this image.

The present x-ray structure determination shows modulated atoms in the *H* layers of $4H_b$-$TaSe_2$ as well. As was explained in Sec. IV B, the participation of the *H* layers in the modulation is required for 3D order of the CDW. Therefore it is to be expected that the *H* layer in $4H_b$-TaS_2 will have a similar modulation. This suggests that the atomic displacements in the *H* layers provide the explanation for the observations by STM. For a better understanding of these observations the tunneling process needs to be considered in more detail. At negative bias ($V_{bias}<0$) electrons tunnel from the metallic substrate towards the tip. Independent of V_{bias} only the electrons at and just below the Fermi level participate in the tunneling process.[16] On further decreasing V_{bias} one thus performs spectroscopy of the density of the empty states of the tip convoluted with the density of states at or near the Fermi level of the substrate. At positive bias the process is reversed, and on increasing V_{bias} one performs spectroscopy of the density of the empty states of the substrate convoluted with the density of states at or near the Fermi level of the tip.

We have determined a modulation in the *H* layers with the same period as the modulation in the *T* layers. This modulation of the atomic positions causes a modulation of the density of states of the electron bands, again with the same period as the period of the *T* layers. However, there is no CDW in the *H* layers, so that the electron states involved in the modulation are not necessarily at the Fermi level. In our opinion they will have energies somewhere in the middle of the unoccupied states of the conduction band. Combining this picture of the electronic states of the *H* layers with the mechanism of STM then shows that at any value of negative bias the local density of states near the Fermi level of the substrate is measured. Since the corresponding electrons have *k* values different from the period of the CDW, a modulation is not observed. On the other hand, for increasing positive V_{bias} the local density of the empty states is scanned. At small values of V_{bias} the modulation will not be seen, while at some larger value of V_{bias} the states with the appropriate *k* values will be involved in the tunneling process and the modulation becomes visible in the STM. The observation by STM of a weak modulation effect at a small negative bias on the *H* layers of $4H_b$-$TaSe_2$ can then be explained by slight differences in the dispersion relations $E(\mathbf{k})$ of the conduction band of the *H* layer for the $X=$S and $X=$Se compounds, respectively.

In order to discriminate with the present direct modulation model and the tunneling model, it would be interesting to measure the bias dependence of the STM images of the *H* layers in $4H_b$-$TaSe_2$. As already mentioned, tunneling cannot explain the observed STM pictures at small negative biases and low temperatures. Increase of the superstructure effect on increasing positive bias then would be a strong indication for our proposed model of the modulation of the local density of the unoccupied states in the *H* layer due to the CDW in the *T* layer.

V. CONCLUSIONS

The $(\sqrt{13}a\times\sqrt{13}a\times c)$ superstructure of $4H_b$-$TaSe_2$ has been determined from x-ray-diffraction data, using a $(3+2)$D superspace description. The principal part of the modulation was found to involve displacements of the atoms of the *T* layers, with Ta forming a lattice of clusters of 13 atoms. This result confirms a CDW on the *T* layers as the origin of the modulation in complete accordance with previous investigations.[3]

The superspace description allowed a direct comparison of commensurate superstructures and incommensurate modulations of different periods. It was thus shown that the modulation of the *T* layers in $4H_b$-$TaSe_2$ is similar to the incommensurate modulation in the nearly commensurate state of $1T$-TaS_2 at room temperature.[11]

A peculiar result of the refinements was that satellite reflections were observed with intensities smaller than that were calculated on the basis of a fully ordered structure model. This discrepancy could be described by a single additional scale factor for all satellites. It was shown that such an effect cannot be due to partial coherence between the two different types of domains, or to a disorder of the stacking of these domains. Instead, it can be explained by disorder of the modulation within single domains, as can be understood

from the weak coupling between consecutive *T* layers due to the presence of intermediate *H* layers.

Small but significant modulation amplitudes were also found for the atoms of the *H* layers, at variance with previous investigations. The relation between the modulations on the *H* and *T* layers suggests that the modulation of the *H* layer is induced by the modulation of the *T* layer, and that a CDW does not exist on the *H* layers. A modulation without CDW is the explanation for the observation of the superstructure by STM on the *H* layers. It was shown that such a simple model can also explain the peculiar bias dependence of STM. Tunneling of electrons through the *H* layers towards the *T* layers is not necessary to explain the observed STM images of the *H* layers.

*Electronic address: jens.luedecke@uni-bayreuth.de

[1] F. Jellinek, J. Less-Common Met. **4**, 9 (1962).
[2] B. E. Brown and D. J. Beentsen, Acta Crystallogr. **18**, 31 (1965).
[3] R. Moret and E. Tronc, Philos. Mag. B **40**, 305 (1979).
[4] W. H. Han, E. R. Hunt, O. Pankratov, and R. F. Frindt, Phys. Rev. B **50**, 14 746 (1994).
[5] J.-J. Kim and H. Olin, Phys. Rev. B **52**, 14 388 (1995).
[6] I. Ekvall, J.-J. Kim, and H. Olin, Phys. Rev. B **55**, 6758 (1997).
[7] J. A. Wilson, F. J. DiSalvo, and S. Mahajan, Adv. Phys. **24**, 117 (1975).
[8] V. Petricek and M. Dusek, computer code JANA96 Prague, 1996.
[9] S. van Smaalen and V. Petricek, Acta Crystallogr., Sect. A: Found. Crystallogr. **48**, 610 (1992).
[10] S. van Smaalen, Crystallogr. Rev. **4**, 79 (1995).
[11] A. Spijkerman, J. L. de Boer, A. Meetsma, G. A. Wiegers, and S. van Smaalen, Phys. Rev. B **56**, 13 757 (1997).
[12] R. Brouwer and F. Jellinek, Physica B & C **99B**, 51 (1980).
[13] M.-H. Whangbo, J. Ren, E. Canadell, D. Louder, B. A. Parkinson, H. Bengel, and S. N. Magonov, J. Am. Chem. Soc. **115**, 3760 (1993).
[14] R. E. Thomson, B. Burk, Z. Zettl, and J. Clarke, Phys. Rev. B **49**, 16 899 (1994).
[15] B. Giambattista, A. Johnson, W.W. McNairy, C.G. Slough, and R.V. Coleman, Phys. Rev. B **38**, 3545 (1988).
[16] S. N. Magonov and M.-H. Whangbo, *Surface Analysis with STM and AFM* (VCH, Weinheim, 1997).